Computational and Structural Biotechnology Journal 21 (2023) 1473–1486

Contents lists available at ScienceDirect

Computational and Structural Biotechnology Journal

journal homepage: www.elsevier.com/locate/csbj

Structural modelling of human complement FHR1 and two of its synthetic derivatives provides insight into their in-vivo functions

Natalia Ruiz-Molina [a,1], Juliana Parsons [a,2], Eva L. Decker [a,3], Ralf Reski [a,b,*,4]

[a] Plant Biotechnology, Faculty of Biology, University of Freiburg, Freiburg, Germany
[b] Signalling Research Centres BIOSS and CIBSS, University of Freiburg, Freiburg, Germany

ARTICLE INFO

Article history:
Received 24 November 2022
Received in revised form 2 February 2023
Accepted 2 February 2023
Available online 3 February 2023

Keywords:
Factor H
Complement factor H-related 1
Complement regulation
AlphaFold
Membrane attack complex
Complement therapeutics

ABSTRACT

Human complement is the first line of defence against invading pathogens and is involved in tissue homeostasis. Complement-targeted therapies to treat several diseases caused by a dysregulated complement are highly desirable. Despite huge efforts invested in their development, only very few are currently available, and a deeper understanding of the numerous interactions and complement regulation mechanisms is indispensable. Two important complement regulators are human Factor H (FH) and Factor H-related protein 1 (FHR1). MFHR1 and MFHR13, two promising therapeutic candidates based on these regulators, combine the dimerization and C5-regulatory domains of FHR1 with the central C3-regulatory and cell surface-recognition domains of FH. Here, we used AlphaFold2 to model the structure of these two synthetic regulators. Moreover, we used AlphaFold-Multimer (AFM) to study possible interactions of C3 fragments and membrane attack complex (MAC) components C5, C7 and C9 in complex with FHR1, MFHR1, MFHR13 as well as the best-known MAC regulators vitronectin (Vn), clusterin and CD59, whose experimental structures remain undetermined. AFM successfully predicted the binding interfaces of FHR1 and the synthetic regulators with C3 fragments and suggested binding to C3. The models revealed structural differences in binding to these ligands through different interfaces. Additionally, AFM predictions of Vn, clusterin or CD59 with C7 or C9 agreed with previously published experimental results. Because the role of FHR1 as MAC regulator has been controversial, we analysed possible interactions with C5, C7 and C9. AFM predicted interactions of FHR1 with proteins of the terminal complement complex (TCC) as indicated by experimental observations, and located the interfaces in $FHR1_{1-2}$ and $FHR1_{4-5}$. According to AFM prediction, FHR1 might partially block the C3b binding site in C5, inhibiting C5 activation, and block C5b-7 complex formation and C9 polymerization, with similar mechanisms of action as clusterin and vitronectin. Here, we generate hypotheses and give the basis for the design of rational approaches to understand the molecular mechanism of MAC inhibition, which will facilitate the development of further complement therapeutics.

1. Introduction

The human complement system is a fundamental part of innate immunity. It builds a surveillance network, which plays a key role in maintaining host homeostasis, contributing to the clearance of dead or modified host cells, and provides the first line of defence against invading pathogens. Complement consists of more than 40 proteins in fluid-phase or associated to the surface of host cells. The complement system is activated in a cascading manner, and this can be initiated by three pathways, the classical (CP), lectin (LP), or alternative (AP) pathway, via proteolysis and/or conformational changes of the involved proteins. These signalling pathways converge at the activation of the very abundant complement component C3 and end up in inflammation, in opsonization of cells, tagging them for phagocytosis, and in membrane attack complex (MAC) formation, triggering lysis (reviewed by [1]).

While the CP and LP are activated upon recognition of invaders, the AP is permanently active in small amounts by spontaneous

* Corresponding author at: Plant Biotechnology, Faculty of Biology, University of Freiburg, Freiburg, Germany.
E-mail address: ralf.reski@biologie.uni-freiburg.de (R. Reski).
[1] ORCID: 0000–0003-1318–6185
[2] 0000–0001-6261–2342
[3] 0000–0002-9151–1361
[4] 0000–0002-5496–6711

https://doi.org/10.1016/j.csbj.2023.02.002

hydrolysis of the constitutively buried thioester bond in C3, leading to C3(H_2O). Generation of C3(H_2O) induces a conformational change of C3 and migration of the thioester-containing domain (TED), leading to a C3b-like molecule, which can bind Factor B (FB), but unlike C3b, it cannot attach to surfaces [2]. C3(H_2O)-bound FB becomes activated by Factor D (FD) to generate a C3 convertase C3(H_2O)Bb in the fluid phase, which cleaves C3 into C3a and C3b. C3a is an anaphylatoxin, which promotes cell recruitment and inflammation. C3b is a central component in the activation cascade and can bind to almost any surface in immediate proximity to the activation site and tag them for phagocytosis, a process known as opsonization, or it can form together with FB the surface-bound convertase C3bBb, establishing the amplifying loop of the AP, and extensively increasing the complement response (reviewed by [3]).

As a consequence of excess C3b, C5 is activated and the terminal pathway is initiated leading to the sequential non-enzymatic assembly of MAC, also known as terminal complement complex (TCC), which builds a lytic pore on membranes. C5 is activated either by cleavage to C5a, a potent anaphylatoxin, and C5b; or without proteolytical cleavage on highly dense opsonized cells, leading to a C5b-like activated C5 [4]. C5b can bind to C6, C7, C8, and C9 building a C5b6–9 arc and leading to polymerization of C9, MAC formation and cell lysis (reviewed by [5]).

As C3b cannot differentiate between foreign- and self-surfaces, cells that are not specifically protected, either by expressing regulators on their surfaces or recruiting them from plasma, can be marked and attacked by the complement system (reviewed by [6]). Therefore, the system is tightly controlled at different levels, in fluid phase and on host cells, to avoid damage of intact body cells, yet allowing efficient clearance of pathogens and damaged cells. Complement regulators typically display pattern recognition regions and binding sites for one or more complement components, and eventually other regulators. As the AP is responsible for 80% of the terminal complement activity [7], regulators of this pathway are of special interest.

Due to the ability of AP C3 convertases to amplify the complement response, their inactivation plays an important role to restrict complement activation to the correct target and appropriate degree. The main regulator in the fluid phase of the AP C3 convertases is Factor H (FH). FH consists of 20 globular domains, the short consensus repeats (SCRs). FH recognizes sialic acids and glycosaminoglycans on healthy host cells, bind them, mainly through SCRs 7 and 19–20 (FH_7 and $FH_{19–20}$), and target its regulatory activity to protect body tissues. $FH_{1–4}$ are able to bind to C3b and compete with FB, thus inhibiting convertase assembly. It can also displace the fragment Bb from the already formed AP C3 convertase, dissociating the complex, an activity known as decay acceleration (DAA). Moreover, FH displays a cofactor activity. When bound to C3b, FH acts as cofactor for the cleavage by Factor I of C3b to inactive C3b (iC3b), and subsequently to C3c and C3dg and finally the latter to C3d. The inactivated fragments are unable to bind FB. However, C3d, which contains the TED domain, can bind to FH through $FH_{19–20}$ [8].

In contrast to the well characterized negative regulatory activity of FH, the mechanism of regulation of the five FH-related proteins (FHRs) is still controversial. FHRs lack the C3b-regulatory region of FH, $FH_{1–4}$, but they share high similarity to the C3d and surface recognition domain $FH_{19–20}$. FHR1 is the most abundant FHR, present in plasma in a similar concentration as FH [9], and of special interest. Due to the C-terminal homology to FH is was proposed to compete with FH for binding to C3b and host cell surfaces, displacing it and leading to local deregulation of complement activation [9]. However, it was recently shown that FHR1's C-terminal domain, with only two substitutions compared to FH, is almost unable to recognize α2,3-linked sialic acids as host surface markers [10,11]. Moreover, in contrast to FH, FHR1 was reported to bind C3, probably recruiting it to promote opsonization [11], and to bind to C5, C6, C7, C8 and C9, inhibiting MAC formation [12,13]. Other inhibitors of MAC assembly include CD59, vitronectin and clusterin. FHR1 displays a dimerization domain in the N-terminal domains ($FHR1_{1–2}$), and it can circulate as homodimer or heterodimer together with FHR2 or FHR5 [9].

Although one of the main functions of the complement system is to protect the body from pathogens, many microorganisms have developed a diverse range of strategies to evade complement attack by, e.g., recruiting soluble complement regulators as a protective shield (reviewed by [1]). On the other hand, over-activation of complement in response to viral infections such as hepatitis C, dengue and coronavirus has been associated with viral pathogenesis [14–17]. Moreover, mutations in complement-associated proteins and deregulation of the activation cascade are associated with a long list of diseases such as age-related macular degeneration, atypical haemolytic uremic syndrome, C3 glomerulopathies, paroxysmal nocturnal hemoglobinuria, and systemic lupus erythematosus. Furthermore, dysregulation of complement activation can contribute to autoimmune and inflammatory diseases [18].

Despite vast efforts, only very few complement-related drugs have reached final regulatory approval. Therefore, there is growing interest in recognizing interactions between complement effectors and regulators, to better understand the role of complement in disease. This knowledge can facilitate the rational development of therapeutics to restore homeostasis in different diseases associated with complement dysregulation.

FH and FHRs could be targets for therapeutic approaches (reviewed by [19]). However, due to the structural complexity of FH, its recombinant production is far from trivial [20,21]. Therefore, smaller proteins including only the main active domains of FH, have been developed [22–24]. More recently, two multitarget fusion proteins, MFHR1 ($FHR1_{1–2}$:$FH_{1–4}$:$FH_{19–20}$) and MFHR13 ($FHR1_{1–2}$:$FH_{1–4}$:FH_{13}:$FH_{19–20}$), were developed, which combine the dimerization and C5-regulatory domains of FHR1 with the C3-regulatory and cell surface recognition domains of FH to regulate the activation of the complement in the proximal and the terminal pathway, and target the regulation to host surfaces. These fusion proteins exhibited a superior overall regulatory activity in vitro compared to FH [13,25,26].

The artificial intelligence AlphaFold2 (AF2) has recently revolutionized structural biology due to unprecedented success and accuracy in protein fold prediction [27]. AF2 is a neural network that uses physical, geometric, and evolutionary constraints. AF2 uses coevolution information from multiple sequence alignments (MSAs) and was further trained to predict protein-protein interactions (PPI) by an algorithm called AlphaFold-Multimer (AFM) [28]. While proteins can adopt different states under specific conditions, only one single state is predicted by AF2/AFM, which is one of the major limitations.

ColabFold was developed based on AF2 and AFM with some modifications, and enables faster prediction in local machines without compromising the accuracy [29]. Benchmarking of AFM showed significantly higher accuracy compared with global docking approaches, with success rates varying between 51 up to 72% [28,30,31]. However, there is still low rate of success for antibody-antigen complexes, probably due to lack of coevolution signals in MSAs (11%) [31]. This is also the case for individual proteins without enough co-evolutionary relationships such as metagenomic protein sequences and viral proteins. Recently a new algorithm was created to overcome these limitations [32].

Here, we studied the structures and interactions of MFHR1 and MFHR13 with different complement components to correlate structural features with previous experimental observations [13]. Furthermore, many structures of MAC regulators and their complexes remain experimentally undetermined. Therefore, we included AFM predictions of the most important MAC regulators, including FHR1, analysed the interactions with MAC components C5, C7 and

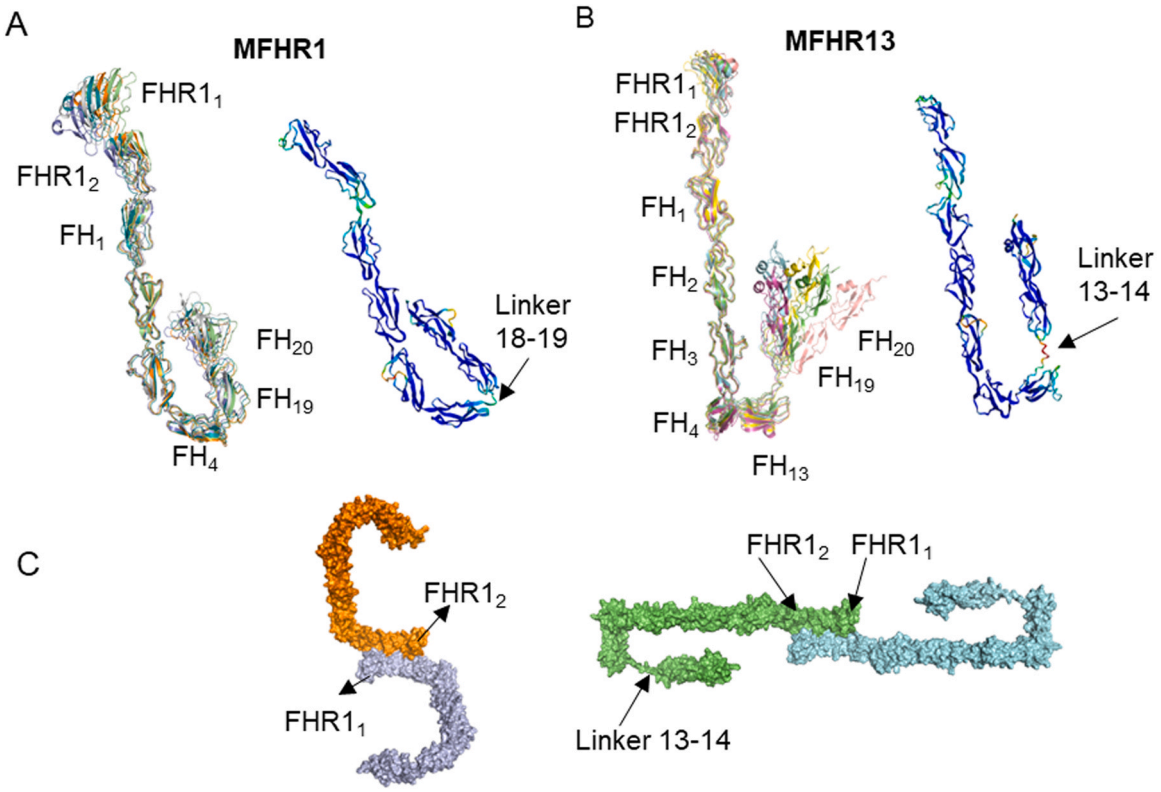

Fig. 1. Structure models of the synthetic complement regulators MFHR1 and MFHR13 predicted by AlphaFold2 (AF2). Structure of MFHR1 top-ranked models (**A**) and MFHR13 (**B**). Superimposition of the 5 top-ranked models are shown in the left panel, while the best model is displayed in the right panel with the pLDDT score (0–100) by colours (> 90 in blue, high confidence, and < 50 in red, low confidence). **C.** Prediction of MFHR1 (left panel) and MFHR13 (right panel) dimerization interface by AlphaFold-Multimer (AFM). The linker between FHR1 and FH domains is also predicted with different possible conformations. (For interpretation of the references to colour in this figure legend, the reader is referred to the web version of this article.)

C9, and generated new hypotheses about the mechanisms of MAC inhibition taking into account previously published experimental results.

2. Results and discussion

2.1. Comparison of MFHR1 and MFHR13 structure models

To further characterize the synthetic complement regulators MFHR1 and MFHR13, we analysed their structure. The rational design of MFHR13 involved originally the modelling of the protein structure using Modeler 9.19 [13]. Here, we used ColabFold based on the AlphaFold2 (AF2) algorithm and AlphaFold-Multimer (AFM) to model both chimeric proteins and evaluate their ability to dimerize.

The AF2 algorithm generated five top-ranked models for MFHR1 and MFHR13. These top-ranked models have a similar conformation and orientation of domains SCRs 19–20 of FH (FH$_{19–20}$) for MFHR1 in contrast to MFHR13 (Fig. 1 A, B, Supplementary Figure 1 A). MFHR13 models differ in the orientation of FH$_{13}$, FH$_{19}$, and FH$_{20}$, probably due to the flexibility of the linkers between SCRs in the C-terminus of the protein. The linker between FH$_{13}$ and FH$_{19}$ in MFHR13, equivalent to the linker between FH$_{13}$ and FH$_{14}$ (13–14 linker) in FH (SMAQIQL), was always predicted with very low confidence (pLDDT < 50), contrary to the linker between FH$_4$ and FH$_{19}$ in MFHR1, which is the natural linker between SCR 18 and 19 (18–19 linker) in FH (EDSTGK). Very low confidence regions predicted by AF2 have been correlated with intrinsically disordered regions (IDRs) [33], which can acquire several conformational ensembles and evolve faster than ordered regions. Furthermore, 13–14 linker in FH is the most variable across species; for instance, the sequences are NEEAKIQL and KEEVLNS in cows and pigs, respectively [34]. Likewise, FH$_{13}$ itself is variable in sequence between orthologues, and the structure differs from the rest of the SCRs. Maximum eight β-strands (named A – H) have been recognized in SCR structures. FH$_{13}$ is the most spherical SCR and lacks β-strand H, along with a three-residue deletion in the flexible loop between β-strands D and E [34]. This loop and the β-strand H are important to stabilize the interface with a consecutive SCR. These unique features indicate that FH$_{13}$ can contribute to the structural flexibility of MFHR13, in agreement with the flexibility predicted by AF2 for the interface 13–19 in this fusion protein.

The quality of the top-ranked model was further evaluated with QMEANDisCo and PROCHECK (Supplementary Figure 1 B, C). QMEANDisCo includes a new distance constraint score based on pairwise distances in the model and constraints obtained from PDB structure homologues to the model. The low score of FH$_{13}$ and the linker might be due to few close homologues with available experimental structures, which decrease the accuracy of QMEANDisCo [35]. The superimposition of PDB structures (PDB 2wii, 2kms, 2xqw) and AF2 prediction with a backbone root-mean-square deviation (RMSD) of 1.37, 0.93, and 1.2 Å for FH$_{1–4}$, FH$_{13}$, and FH$_{19–20}$, respectively, indicates that they are quite similar to the experimental structures (Supplementary Figure 2 A). Furthermore, AFM correctly predicted the dimerization interface in FHR1$_{1–2}$ on both synthetic regulators compared with an experimental structure of FHR1$_{1–2}$ (PDB 3zd2) (Fig. 1C), although the prediction quality was not highly confident (Supplementary Figure 2 B).

2.2. Binding of MFHR13, MFHR1 to C3 and C3 cleavage fragments

C3 consists of two chains (α and β), containing 13 domains; eight of them with a fibronectin-type 3-like core fold, called macroglobulin (MG) domains. A series of proteolytic reactions results in

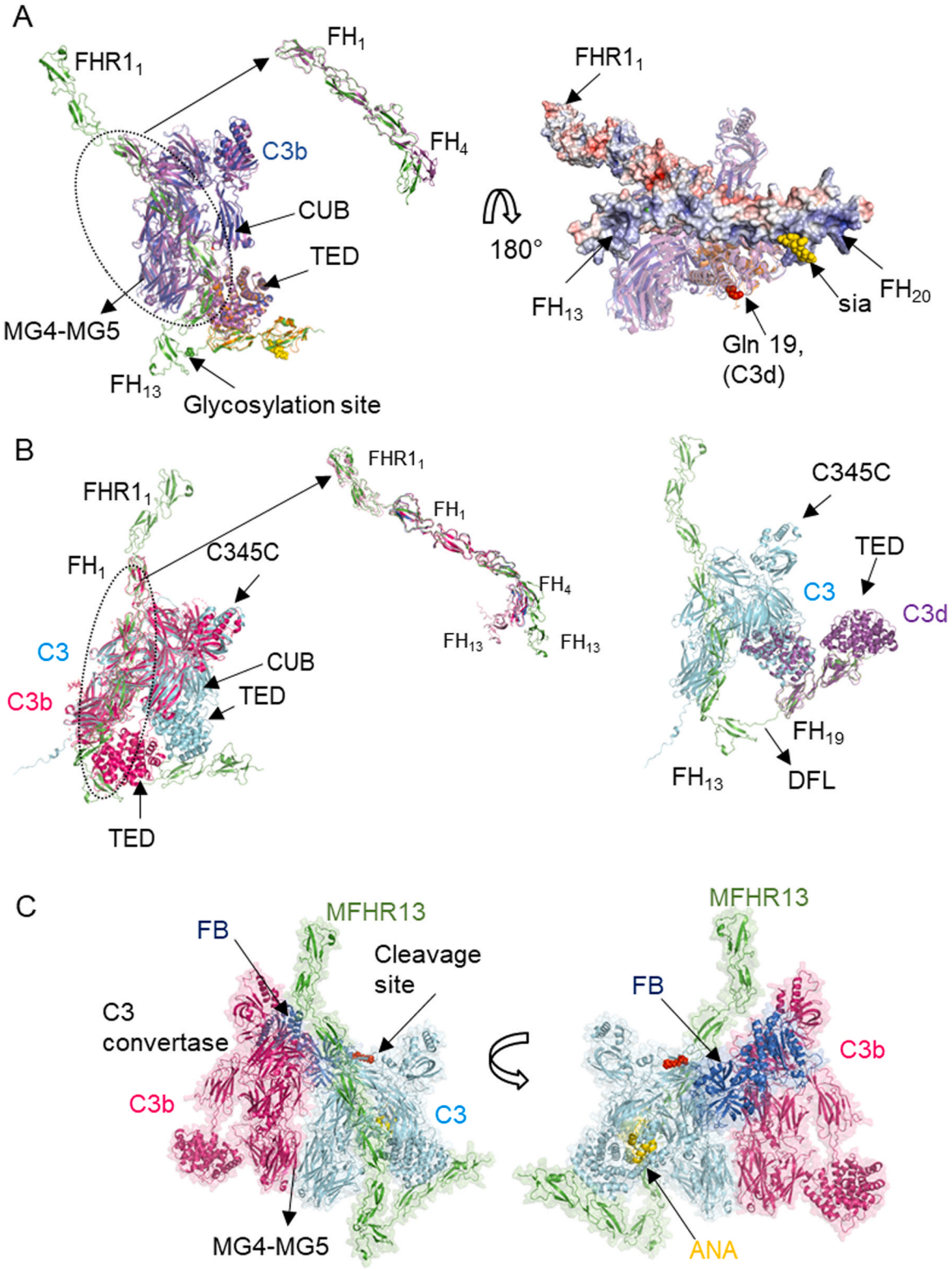

Fig. 2. Interaction of MFHR13 with C3 and C3b predicted by AlphaFold-Multimer. **A.** The model of the complex MFHR13/C3b predicted by AFM agrees with experimental structures of FH fragments in complex with C3b. Superimposition of the model MFHR13 (green) interacting with C3b (blue) with experimental structure of FH_{1-4}/C3b (magenta) (PDB 2wii, RMSD = 1.253 Å), FH_{19-20}/C3d (orange) (PDB 2xqw, RMSD = 0.928 Å) and sialic acid (yellow) (PDB 4ont), (RMSD = 1.253 Å). The thioester-containing domain (TED) and complement C1r/C1s, Uegf, Bmp1 domain (CUB) are indicated by arrows. Zoom in of the superimposition of FH_{1-4} of the model and the experimental structure is shown. The right panel shows the linkage of C3b (or C3d) to biological surfaces around Gln19 (red spheres) and MFHR13 as a surface with the electrostatic surface potential (electropositive residues in blue and electronegative in red). **B**. MFHR13 interacts with C3 through FH_{1-3} and FH_{19} domains. On the left, MFHR13 and C3 are shown in green and cyan, respectively, and the model is superimposed with C3b in complex with FH_{1-4} (PDB 2wii, in magenta), where differences in C3 and C3b conformations are observed. RMSD is 2.583 Å for the whole complex superimposed with PDB 2wii, and 1.376 Å for FH_{1-4}, respectively. The right panel shows superimposition of MFHR13/C3 model (green/cyan) with experimental structure FH_{19-20}/C3d (PDB 2qxw, in purple). RMSD is 0.601 Å for C3 TED domain and C3d. The disordered flexible linker (DFL) is shown. **C.** C3 convertase (C3bBb) in complex with C3/MFHR13 (enzyme-substrate complex). Superimposition of C3 in MFHR13/C3 model with MG4-MG5 domains of C3b molecule in C3 convertase (PDB 2win, C3b in magenta, Bb fragment in dark blue). MFHR13 is shown in green and C3 in light blue with the anaphylatoxin domain (ANA) in yellow and the cleavage site as red spheres. (For interpretation of the references to colour in this figure legend, the reader is referred to the web version of this article.)

several C3 fragments with different functional properties. These fragments are derived from the α-chain while the β-chain remains intact. MG1-MG5 and part of MG6 form the β-chain with a linker domain. The α-chain is formed by an anaphylatoxin domain, part of MG6, along with MG7, MG8, a thioester-containing domain (TED), complement C1r/C1s, Uegf, Bmp1 domain (CUB), and the C-terminal domain, called C345C [36]. The anaphylatoxin domain forms C3a when C3 is cleaved by C3 convertases, and the TED domain forms C3d when C3b is cleaved for inactivation, and allows covalent attachment of C3b and C3d to cell surfaces (opsonization).

It is well known, that FH can bind C3b through FH_{1-4} or FH_{19-20} and regulate complement activation [37]. In order to delineate a probable mechanism for the synthetic regulators MFHR1 and MFHR13, we evaluated their binding to C3b using AFM and compared it to the experimental structures of FH_{1-4}/C3b (PDB 2wii), FH_{19-20}/C3d (PDB 2xqw), and FH_{18-20}/C3d (PDB 3sw0). AFM predicted the interaction between MFHR13 and C3b with interfaces located in FH_{1-4} and FH_{19} (Fig. 2 A) in agreement with experimental structures of FH fragments [8,38]. According to the model, both sites might be used simultaneously to bind one C3b molecule, while these binding sites are considered independent in FH [23]. The ability to bind simultaneously to one C3b molecule can have an impact on the functional activity of the protein as a potential therapeutic agent, which will be further discussed. The experimental structure of FH_{1-4}/C3b and the model of MFHR13/C3b are highly similar with an RMSD of 1.253 Å, but the orientation of FH_4 is slightly different (Fig. 2 A, zoomed panel). The linkers in FH_{1-4} have some degree of inherent flexibility and it has been shown that a kink between FH_3 and FH_4 occurs when they bind C3b [37]. An additional C3b binding site in FH was suggested to be located in FH_{13-15}, which binds with a weak affinity [39], however none of the analysed models predicted a binding site localized in FH_{13} in MFHR13.

We compared the models of MFHR1 and MFHR13 in complexes with C3b. Although AFM predicted the correct interfaces for C3b binding on FH_{1-4} and FH_{19-20}, the differences in flexibility of the 18–19 linker in MFHR1, and the 13–14 linker in MFHR13, respectively, determine if the binding to one C3 or C3b molecule occurs independently or simultaneously via both interfaces. The model of MFHR1 in complex with C3b showed a different orientation of FH_4 and FH_{19} compared with FH_{18} and FH_{19} in the crystal structure FH_{18-20} (PDB 3sw0) (Supplementary Figure 3 A). Probably, the conformation of FH_{18-19} in the experimental structure (PDB 3sw0) is just one of several possible conformations, since the 18–19 linker is significantly more flexible than the19–20 linker [40]. Moreover, a mini-FH version with an optimized artificial linker (12 glycines) outperformed the original version with the natural linker 18–19 in an overall alternative pathway regulation assay, which was attributed to the inability of the original molecule to bind simultaneously to one C3b molecule using both interfaces [41]. We conclude that in MFHR1 the simultaneous interaction of one C3b molecule with both interfaces (FH_{1-4} and FH_{19}) is theoretically possible, although the short length of the 18–19 linker can impose some constraints, which could be overcome by the use of an optimized linker. Although there was no experimental difference between MFHR1 and MFHR13 in C3b binding in vitro by an ELISA-based method [13], other approaches like Surface Plasmon Resonance (SPR) or Biolayer interferometry (BLI) should be evaluated to determine the differences in association and dissociation rate to C3 and its fragments.

It is important to highlight that AFM predicted a simultaneous binding between C3b and MFHR13 or MFHR1 through both interfaces only by using templates. The amount of recycles plays an important role as it was previously described [31] and up to 15 or 8 recycles were needed for MFHR1 and MFHR13, respectively, otherwise only one of the interfaces were predicted. The Inter-PAE for the models are shown in Supplementary Figure 3 B.

According to the model, when MFHR13 binds to surface-bound C3d or C3b, the electropositive patch between FH_{13} and FH_{20} is oriented towards the surface to bind GAGs or sialic acid, leaving the active domains to regulate complement on host cell surfaces (Fig. 2 A, right panel). We observed a higher binding to heparin which is correlated with the presence of FH_{13} in MFHR13 compared with MFHR1 [13].

While FH cannot bind C3, it was recently shown that FHR1 binds C3, C3b, iC3b and C3d [11]. Therefore, we included C3 as a potential ligand of MFHR13 and MFHR1. AFM without templates predicted an interaction of C3 with interfaces located in FH_{1-3} and FH_{19} of MFHR13 and MFHR1 (Fig. 2 B, Supplementary Figure 3 C, D). The interaction between FH_4 and the TED domain, which occur in the complex FH_{1-4}/C3b (PDB 2wii) [42], might be prevented in MFHR13 due to conformational differences between C3b and C3, specifically in the C345C and TED domains (Fig. 2 B). C3-binding sites in FH might be cryptic and thus FH cannot bind C3. However, the fragment FH_{1-6} binds C3, but only with 5-fold weaker affinity compared to FH/C3b [39], which is in agreement with the AFM prediction. Thus, we propose that in contrast to FH, but similar to FHR1 or FH_{1-6}, MFHR13 and MFHR1 might bind to C3 due to their extended conformation in fluid phase. As opposed to MFHR13, it is unlikely that MFHR1 can interact with one C3 molecule simultaneously through the interfaces predicted in FH_{19-20} and FH_{1-3}, since the 18–19 linker would need to acquire a complete extended conformation (Fig. 2 B, Supplementary Figure 3 C).

Although AF2 has an outstanding ability to predict global protein structures, the accuracy decreases significantly for multi-domain proteins compared to individual domains [43,44]. Therefore, inter-domain orientation in models of MFHR13, MFHR1, FH and FHR1 should be interpreted with caution. MFHR13 structure models showed always a similar orientation of FH_3, FH_4 and FH_{13}. However, in complex with C3 ligands, the orientation of FH_4 with respect to FH_3 changed slightly, along with the flexible 13–14 linker which acquired an extended conformation to allow the simultaneous binding to one C3 molecule through both interfaces (FH_{1-4} and FH_{19}) (Fig. 2 A, B). Although an extended linker conformation would not be reliable, this linker is likely to be a disordered flexible linker (DFL) according to the pLDDT as mentioned above. Despite other approaches such as IUPred2A, DISOPRED3, fMoRFpred, DFLpred and TransDFL failed to predict this linker as a disordered region (Supplementary Figure 3 E), a previous study showed that AF2 exceeded the performance of 11 disordered region predictors on the DisProt-PDB dataset [45].

The cofactor activity is essential for complement regulation since C3b is inactivated to prevent C3 depletion, additional C3 convertases formation and C3b deposition on cell surfaces [46]. FH and the synthetic regulators MFHR1 and MFHR13 act as cofactor for factor I (FI), a serine protease, which circulates in an inactive form. The interactions between FI, C3b and FH are fundamental to trigger the remodelling of the active site [47]. Different mini-FH versions exhibited lower cofactor activity in fluid-phase than full-length FH [22,48], as it is the case for MFHR1 and MFHR13. [13,25,26]. According to AFM models we speculate that a high entropy in MFHR13 due to the 13–14 linker might destabilize the interaction between C3b and FH_4 when FH_{19} is interacting simultaneously with the TED domain of C3b. Although FH_4 in FH is not directly interacting with FI as FH_{1-3} is, FH_4 interaction with C3b might hold the TED domain position while the CUB domain is cleaved [37]. In contrast, this conformation of FH_4 would not affect decay acceleration activity (DAA) because the interaction of FH_{1-2} with C3b can displace the Bb protease fragment (by electrostatic repulsion), while the other interactions of FH_{3-4} and even the FH_{19} can support the binding to C3b to improve the DAA. This might explain why MFHR13 was better than MFHR1 in DAA [13], since the simultaneous binding to C3b is more feasible than for MFHR1.

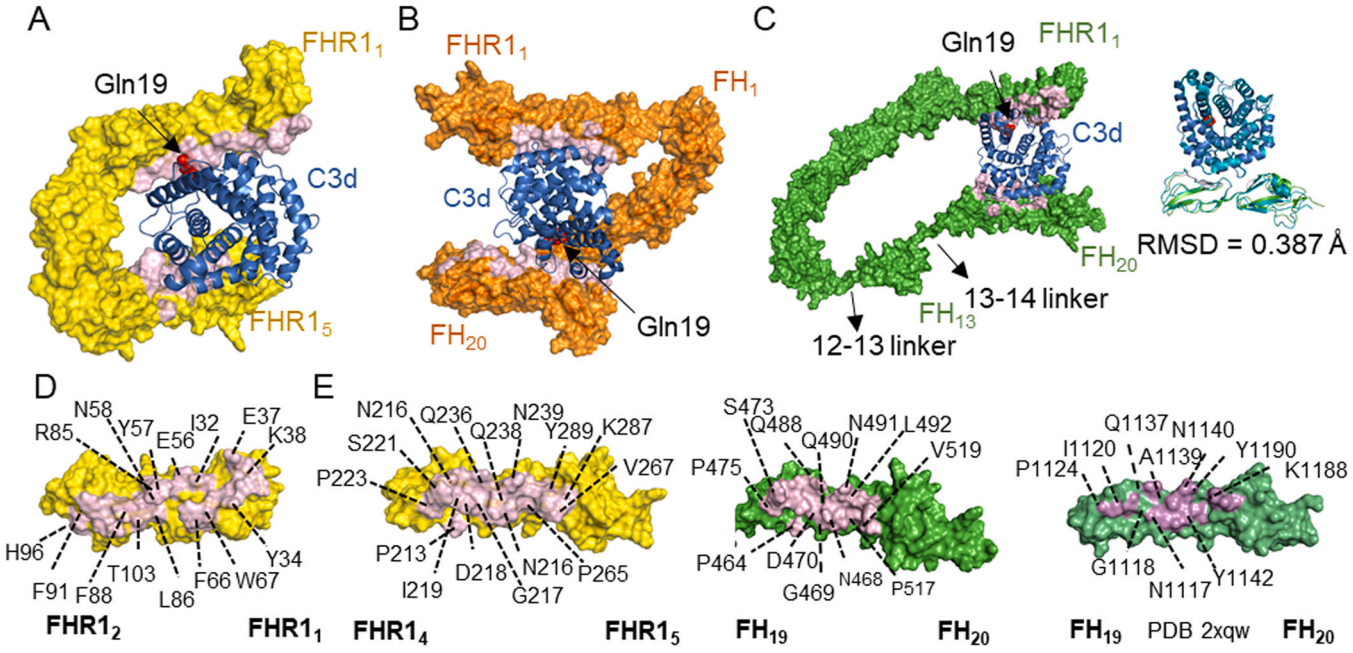

Fig. 3. Interactions of FHR1, MFHR1 and MFHR13 with C3d predicted by AlphaFold-Multimer. **A.** FHR1 interacts with C3d through FHR1$_{4–5}$ with high confidence score while a second interface in FHR1$_{1–2}$ was predicted overlapping the C3d region linked to biological surfaces around Gln19 (shown as red spheres in all structures). MFHR1 **(B)** and MFHR13 (**C**) interact with C3d through FH$_{19–20}$ with a high confidence score. The same interface in FHR1$_{1–2}$ was identified for these proteins **D**. Binding interface (in pink) between FHR1$_{1–2}$ and C3d with some residues labelled in FHR1. **E.** Binding interfaces between FHR$_{4–5}$ (left side) and FH$_{19–20}$ with C3d predicted by AFM without templates (center) compared with the experimental structure PDB 2xqw (right side). Some residues in the interface are labelled in FHR1 and FH. (For interpretation of the references to colour in this figure legend, the reader is referred to the web version of this article.)

The ability of MFHR13 and MFHR1 to bind C3 as predicted by AFM might have implications for complement regulation that should be carefully considered. Surface-bound FHR1 can bind C3b, allowing convertases assembly by displacing FH, and it can also bind to C3, increasing its local concentration, generating more C3b and in turn triggering complement activation instead of negatively regulating it [11,49]. MFHR13 can bind C3 not only through the TED domain as FHR1 does. Therefore, to check if MFHR13 binding to C3 avoids its cleavage by C3 convertases, we created a hypothetical model of C3 convertase interacting with C3 as described by [50]. MFHR13 bound to C3 would not interfere with the interaction of C3 and C3 convertases whose interface is located in MG4-MG5 domains. Thus, it would not prevent cleaving additional C3 into C3b, similar to what was shown for FHR1 variants [10] (Fig. 2 C). Once C3b is generated, MFHR13 can act as cofactor for FI to inactivate C3b to iC3b, thus counteracting complement activation, which is not possible for FHR1. Although it applies also for MFHR1, the affinity of both synthetic regulators to C3 should be determined experimentally. Even if both proteins perform well as complement regulators in vitro, these characteristics should be considered to evaluate different performances in vivo.

Previously, we also analysed the binding to C3d, an inactivated C3b fragment, which is important for MFHR1 and MFHR13 to target the therapy to regions with ongoing complement activation [13]. It is well known that FHR1 and FH bind C3d through FHR1$_{4–5}$ [51] and FH$_{19–20}$ [8], respectively. AFM without templates correctly predicted the interacting interfaces between C3d and those domains in FHR1, MFHR1, or MFHR13 with a good confidence score (Fig. 3 A, B, C), although always lower for the synthetic regulators (Supplementary Figure 4). Additionally, AFM predicted an interface located in FHR1$_{1–2}$, which is also present in the synthetic regulators (Fig. 3 A, B, C, D). However, the corresponding interface on C3d would be blocked since it is linked to biological surfaces through a region around Gln19. Therefore, it might not be physiologically relevant and it is predicted with a lower score compared to FHR1$_{4–5}$ (Supplementary Figure 4). Furthermore, the extended conformation of 12–13 linker in MFHR13 is not reliable, since it is a not flexible linker [34] therefore the protein might not interact simultaneously with one C3d molecule using both interfaces. The interface in FH$_{19–20}$ coincides with the experimental structure (PDB 2xqw), and more residues in the interface FH$_{19–20}$ are interacting in AFM models as in the experimental structure, which derived from the position of the lateral chains (Fig. 3 E).

2.3. Interactions between FHR1 and terminal complement components

The terminal pathway of complement activation leads to MAC formation, which builds a pore on the cell membrane triggering lysis of pathogens. MAC consists of C5b, C6, C7, the heterotrimeric C8 (C8αβγ) and around 18 C9 molecules [5]. The ability of FHR1 to bind C5 has been a matter of controversy [9,12]. Recently, we observed binding of FHR1 as well as the synthetic proteins MFHR1 and MFHR13 to C5 and other components of the MAC. Moreover, in molar excess they were able to inhibit activation of the terminal pathway and cell lysis in a haemolytic test [13]. This indicates a role of FHR1 in regulating MAC formation.

AFM predicted successfully the interfaces of MFHR1, MFHR13 and FHR1 with C3, C3b and C3d. Further, we modelled their complexes with C5, C7 and C9 to evaluate whether the structures can provide insights into the molecular mechanism of MAC inhibition. Vitronectin (Vn) and clusterin are important soluble regulators of the MAC, and CD59 is the only regulator anchored to the membrane and is found on almost all tissues. How the MAC regulators work is still subject of several studies but no crystal structures are available. Therefore, we included models of these regulators in our analysis.

The models were run using amber algorithm to place the side chains, with 3, 6, 12 and 20 recycles with and without templates and the 5 top ranked models predicted by AFM were analysed for each run.

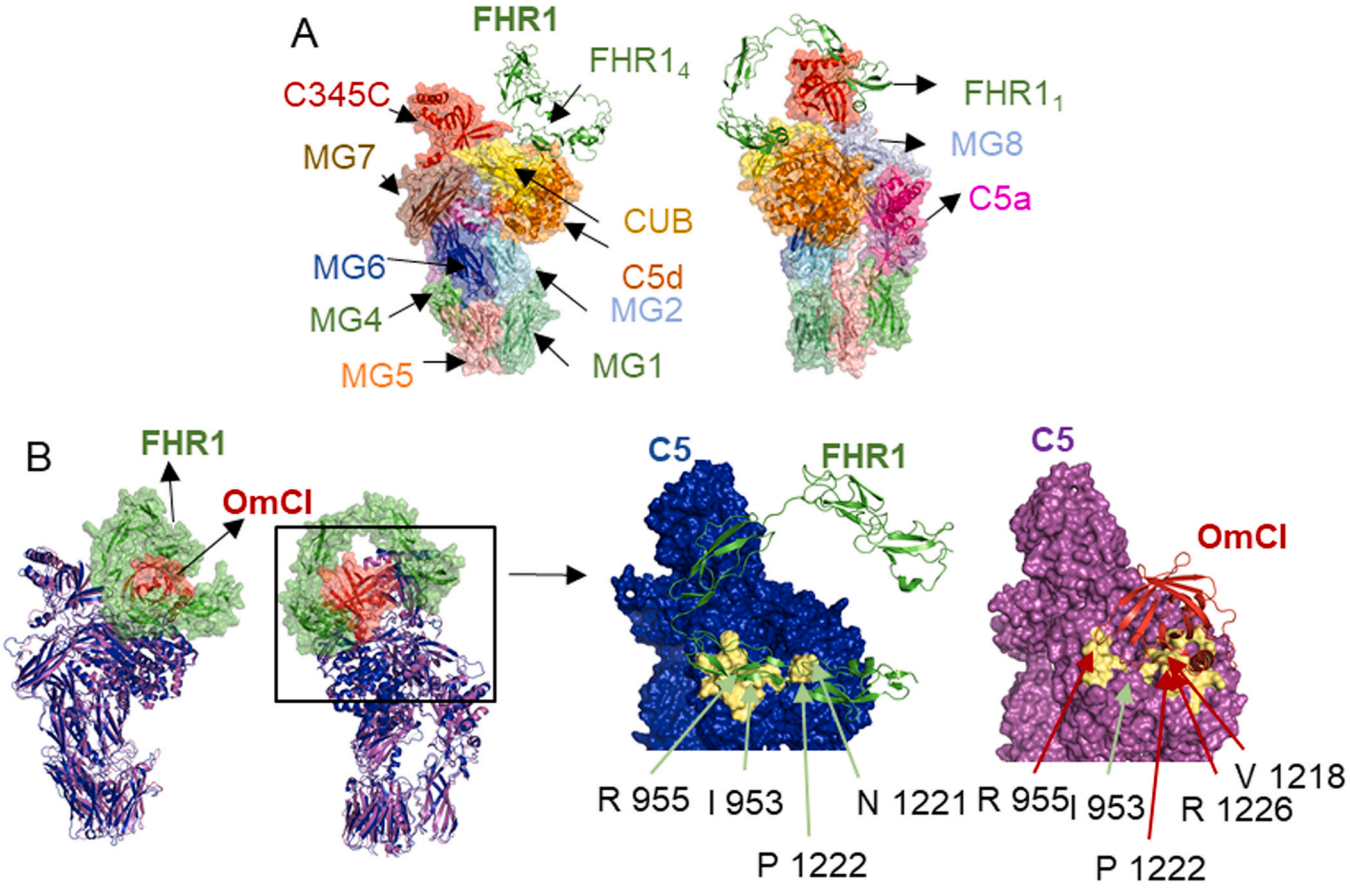

Fig. 4. Interaction of C5 and FHR1 predicted by AlphaFold-Multimer. **A**. Model of FHR1/C5 complex predicted a binding interface in CUB and C5d domains. The colours of C5 domains; shown as surface, match the colour of their legends and FHR1 is shown as cartoon (green). **B**. Model of FHR1/C5 complex indicates a binding interface in the CUB and C5d domains, similar to complement inhibitor OmCI. Superimposition of the model FHR1/C5 predicted by AFM (C5 cartoon in blue, FHR1 surface in green) and C5 in complex with OmCI (PDB 6rqj) (C5 cartoon in purple, OmCI surface in orange), (RMSD = 0.742 Å). The right panel show the binding interfaces of FHR1/C5 and OmcI/C5 in pale yellow with key residues indicated by green or red arrows, respectively. (For interpretation of the references to colour in this figure legend, the reader is referred to the web version of this article.)

2.3.1. Interactions between FHR1 and C5

Similar to C3, C5 consists of 11 domains, 8 MG domains, the anaphylatoxin C5a, CUB domain, TED domain (C5d), and the carboxy-terminal C345C domain, which is flexibly attached to the C5 core (Fig. 4). After activation, C5b and C5b-like are not stable (the half-life of C5b is around 2 min) and C6 should quickly bind to form a stable complex, C5b6, which is the first step in MAC formation [52]. The C5d domain interacts extensively with C6 to form C5b6 and, unlike C3b or C3d, C5b cannot covalently attach to cell surfaces through the TED domain, since it does not contain an internal thioester bond but a structurally homologue of the TED domain of C3 [53].

The top ranked AFM model predicts FHR1 interaction with C5 through interfaces located in FHR1$_{4–5}$, where mainly 7 residues are involved forming 10 hydrogen bonds (Fig. 4 A, Supplementary Figure 5). This binding interface was unexpected since the N-terminal region of FHR1 has been suggested to bind C5 [12]. The top key residues predicted in the interface were Phe 222, Tyr 289, Gln 238, Gln 236, Thr 220, Pro 223 in FHR1 and Arg 955, Ile 953, Pro 1222, Phe 1352, Asn 1221, Thr 952 in C5. According to the AFM model, FHR1 would not bind near convertase-binding site in C5 MG4-MG5 domains. Therefore, FHR1 would not interfere with convertase binding by steric blocking. However, the model shows a similar binding interface as the complement inhibitor OmCI (Coversin, Nomacopan), isolated from the tick *Ornithodoros moubata*, which is currently under clinical trials to treat several complement-associated diseases [54]. This 16-kDa protein binds a region of C5 CUB and C5d and there is one amino acid involved in the C345C domain [52] (Fig. 4 B). C5d-CUB-MG8 domains undergo a conformational rearrangement after proteolytic cleavage of C5 to C5b or non-proteolytic C5 activation, which is critical for C6 binding [4,53]. It has been proposed that OmCI generates an allosteric modulation of convertases, reducing the affinity or blocking the binding of these to C5 [55]. Furthermore, the interaction with one residue in C345C seems to be critical for OmCI's role as complement inhibitor [52]. Interestingly, in our models there is no FHR1 interaction with this domain.

According to the AFM model, FHR1 binds CUB and C5d domains with a smaller interface compared to OmCI (Fig. 4 B), which binds to C5 with a high affinity constant (K_d) in the low nanomolar range [56]. MFHR13, on the other hand, binds C5 with a K_d in the low micromolar range [13], what might limit its activity on C5 level to elevated local concentrations of activated C5.

The molecular mechanism of proteolytic and non-proteolytic C5 activation is not well understood. C5 activation occurs on cell surfaces with C3b deposition, where interactions between C5 and C3b are critical. According to [4], C3 convertases cleave C5 in presence of additional C3b molecules. Experimental structures of C5 in complex with C3b are not available, but the structure of C5 in complex with cobra venom factor (CVF), a C3b homologue, suggests that C5 interacts directly with C3b, also as part of C3 convertases, through MG4-MG5 domains, similar to the C3 convertase in complex with C3 [57]. Other suggested binding sites for C3b are located in the C5 CUB domain [4]. Therefore, according to the AFM predicted model, we propose that binding of FHR1 to C5 might partially block C3b binding, inhibiting in turn C5 activation, which should be experimentally validated.

2.3.2. Interactions between FHR1 and C7

C7 initiates the MAC assembly by binding to C5b6, forming C5b-7 which can attach to membranes and can recruit C8. C7 is a limiting factor in MAC assembly as it is the only TCC protein which is not mainly produced by hepatocytes [58] and C8 is an inhibitor of the MAC assembly itself because it can prevent the insertion into the membrane if it binds to C5b-7 before the insertion occurs [59].

C7 consists of nine domains, two thrombospondin-type domains (TSP type 1), a lipoprotein receptor class A domain (LDLRA), a membrane attack complex-perforin domain (MACPF) (also present in C6, C8 and C9), an epidermal growth factor (EGF) domain, and at the C-terminus of C7 there are two short-consensus repeats (SCRs) and two factor I-like membrane attack complex (FIM) domains which interact with C5b in the assembled MAC [60,61]. MACPF is responsible for the β-barrel pore formation containing a helix-turn-helix (CH3) motif and two amphipathic transmembrane β-hairpins (TMH1, TMH2), while the rest act as auxiliary domains interacting with C6 or C8. Top-ranked models predicted by AFM show three potential binding interfaces between FHR1 and C7. However, the interface predicted with the highest score confidence is located in SCR1 and SCR2 of C7 comprising 20 residues (around 604–681), and 11 and 8 residues in $FHR1_4$ and $FHR1_5$, respectively (Fig. 5 A, B, Supplementary Figure 6 A) forming 10 strong hydrogen bonds. Key residues in the interface include Arg 314, Thr 220, Phe 222, Asp 218 and Arg 291 in FHR1 and Ser 675, Ile 606, Gln 627, Ile 629, Ser 676 in C7.

According to superimposition of the AFM model with the model derived from cryoEM reconstructions of C7 in soluble MAC [61], the binding sites do not overlap with C8 binding sites in the C5b-7 complex (Fig. 5 C). However, FHR1 binding sites overlap partially with C5b-C7 interfaces, which suggest that FHR1 binding to C7 would prevent the formation of the C5b-7 complex (Fig. 5 C). It is important to highlight that FHR1-MAC interacting interfaces overlap partly with the C3d binding region.

This mechanism of action is similar to those observed for clusterin and vitronectin, the most important soluble regulators of the MAC. These proteins bind to TCC proteins and according to affinity assays on lipid bilayer, Vn prevents the binding of C5b-7 to the membrane, while clusterin binds to it without blocking the membrane association site [62]. These multifunctional proteins have large disordered regions and, due to their flexibility, the tertiary structure could not be experimentally determined. Therefore, the molecular mechanism by which Vn and clusterin recognize and block the MAC is not well understood [61]. Here, we analysed whether AFM can predict interactions between Vn and C7 and compared them with FHR1. The top ranked models across different runs with several recycle numbers show a clear interaction interface between C7 and Vn (Fig. 5 C, Supplementary Figure 6 B). Different potential binding interfaces were found, which agrees with a previous study, in which several Vn molecules were identified cross-linked in soluble MAC by combining cryoEM and cross-linking mass spectrometry (MS) [61]. According to our models, none of the interfaces were predicted in the heparin-binding region (362–395) of Vn, as was initially postulated [63] and contradicted later [64]. In the AFM model, the largest interface was located in a part of hemopexin 3–4 domains of Vn and a region of C7 MACPF (around residues 166–306) with 27 and 32 residues interacting, respectively, 17 strong hydrogen bonds, 4 hydrophobic interactions, 4 salt bridges and 2 electrostatic interactions. A hydrophobic cluster was identified with an area of 965.9 $Å^2$ comprising 20 residues and 2.2 contacts/residue. Residues involved in the hydrophobic cluster are Leu 319, Leu 320 and Ile 316 in vitronectin and Ile 263 and Leu 184 in C7 (Supplementary Figure 6 C). The key residues in the interface are Lys 420, Ile 263 and Ser 185 in C7, and Arg 330 and Leu 319 in Vn, involved in salt-bridges and hydrophobic interactions.

The second interface between Vn and C7 is located in part of hemopexin 1–2 of Vn and the first factor I-like membrane attack complex domain (FIM 1) of C7 with 17 and 18 interacting residues, respectively, forming 14 strong hydrogen bonds, 2 hydrophobic interactions, 5 salt-bridges and 3 additional electrostatic interactions (Supplementary Figure 6 B). Some key residues in the interface are Arg 712, Arg 753, Met 717 in C7, and Asn 169, Trp 322, Asp 232 in Vn, involved in hydrogen bonds, salt-bridges and hydrophobic interactions.

Recently, it was suggested that FIM 1 of C7 is responsible for the adaptation of C5b to enable the complete MAC assembly, since it can reorient the C5b C345C domain and triggers the accommodation of macroglobulin domains MG4 and MG5 of C5b to recruit C8β [61]. According to our models, interaction of Vn with FIM1 of C7 would avoid the binding of C7 to the C5b C345C domain in C5b6, hindering its activation. Likewise, the second Vn-binding site in C7 MACPF, overlaps in a small part with the region that undergoes a conformational change to form transmembrane β-hairpins and insert into the membrane. Binding of Vn to this site might avoid the conformational change of C7 to penetrate the membrane and interfere with C6 binding, preventing C5b-7 complex formation and membrane insertion (Fig. 5 C, Supplementary Figure 6 D). New binding sites between Vn and C5b-7 complex might be formed after dramatic conformational rearrangements of C7, C5 and C6 that are not predicted by AFM. Moreover, there are additional binding sites in C5b and C6 in the complex C5b-7 with Vn shown by combining cryoEM and cross-linking MS [61], which might be important for soluble MAC clearance and regulation of C5b-8 complex formation.

Although the binding sites on C7 for FHR1 and the hemopexin 1–2 and 3–4 domains of vitronectin are different, the mechanism of action would be similar, avoiding the formation of a C5b-7 complex. Reports about correlation between protein-protein interactions derived from the structure and their binding affinity are limited, however, a moderate correlation was shown for features such as number of H-bonds and geometric complementarity [65]. The predicted interacting interfaces with C7 are larger for Vn than for FHR1 and could explain why vitronectin is one of the main regulators found associated to soluble MAC and might correlate with a higher binding affinity.

2.3.3. Interactions between FHR1 and C9

The binding of C9 to C5b-8 is the kinetic bottleneck of MAC formation, followed by rapid unidirectional polymerization of additional C9 to build a circular pore [59].

The models for the analysis of the interaction between C9 and FHR1 were predicted by AFM with several recycle numbers, amber relaxation and with or without templates. Top ranked models suggest interactions between C9 and FHR1 with interfaces located in domains $FHR1_{1-2}$, $FHR1_5$ and a small region in $FHR1_4$, involving 10, 14 and 3 residues, respectively (Fig. 6 A, Supplementary Figure 7 A). The $FHR1_{1-2}$ binding interface forms 10 hydrogen bonds and 8 hydrophobic interactions, while the $FHR1_{4-5}$ binding interface forms 17 hydrogen bonds, 9 electrostatic interactions and 4 hydrophobic interactions. The key residues in the top-ranked model predicted by AFM identified by MM-GBSA implemented in HawkDock server were Phe 66, Glu 294, Tyr 34, Arg 302, Trp 282, Glu 297, Tyr 57, Gln 242, and Ser 65. Both binding sites are located in a region of the C9 MACPF domain (Fig. 6 A, B). As mentioned above, it is still difficult to predict the correct orientation of FHR1 domains, therefore, FHR1 might interact simultaneously or independently through several binding regions with C9.

The binding sites in $FHR1_{1-2}$ coincide with the dimerization interface of FHR1. Therefore, binding to C9 would compete with the dimerization of FHR1. The C9-binding interface in $FHR1_{4-5}$ differs from the binding interface to TED domain of C3 (or C3 fragments). However, FHR1 cannot bind both molecules simultaneously due to steric hindrances and clashes (Fig. 6 B). To explore the effect of FHR1 and C9 interaction on MAC formation, our models were

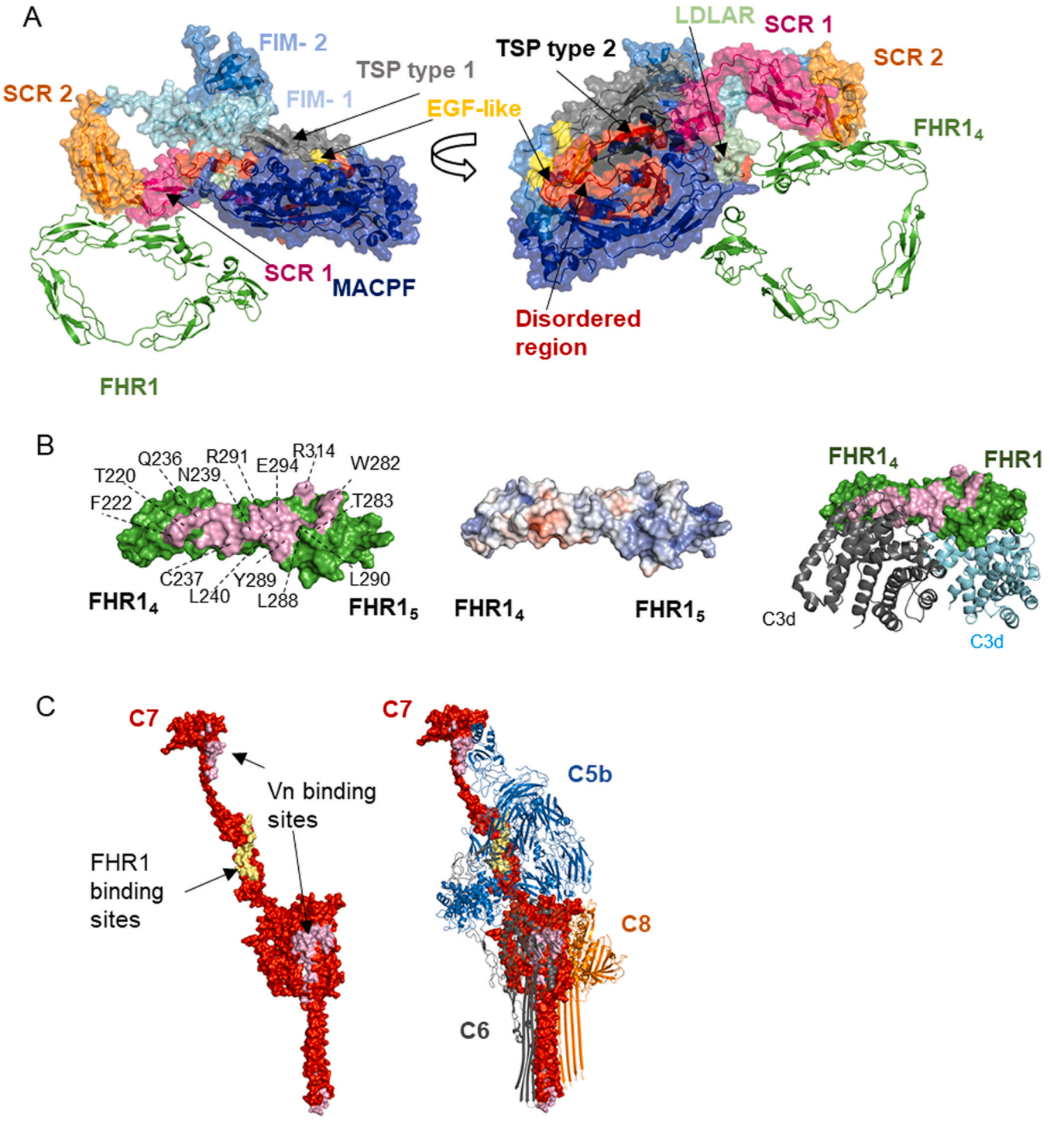

Fig. 5. Interactions between FHR1 and C7 predicted by AlphaFold-Multimer. **A.** FHR1$_{4–5}$ interacts with SCRs 1–2 domains of C7 according to top-ranked AFM model. The colours of nine C7 domains, shown as surface, match the colour of their legends and FHR1 is shown as cartoon in green. **B.** Binding interfaces in FHR1 of the model presented in A (left panel) with electrostatic potential surface (middle panel, electropositive residues in blue and electronegative in red). Some of the residues forming the binding region of FHR1 are labelled (interface shown in light pink). The binding region in FHR1$_{4–5}$ partly overlaps with C3d binding region (right panel). (Experimental structures of C3d/FHR1$_{4–5}$, PDB 3rj3). **C.** FHR1 and vitronectin binding to C7 would interfere with C5b-7 complex formation. The C7 interacting interfaces with FHR1 and Vn are marked in pale yellow and purple, respectively, on the experimental C7 structure in the soluble MAC (PDB 7nyc). The complex C5b-8 is shown with C7 as a surface and C5b, C6, C8 as cartoon. (For interpretation of the references to colour in this figure legend, the reader is referred to the web version of this article.)

superimposed with a structure of the C5b-8 and C5b-9 complex. The best model predicted by AFM indicates FHR1 binding to a C9 MACPF region which does not undergo conformational changes upon C9 binding to C5b-8, indicating that FHR1 can also bind to monomeric C9 in MAC. Furthermore, FHR1 would block C9 polymerization, since the binding region with the C9 monomer coincides with C9-C9 polymerization interface (Fig. 6 C). The interaction between FHR1 and native/soluble C9 would block binding to the C5b-8 complex (Fig. 6 C).

Clusterin and vitronectin can bind to C9, and block its polymerization and pore formation [64,66]. Clusterin binds to pre-complexes C5b-7, C5b-8, C5b-9 but not to C5b6, and it binds to

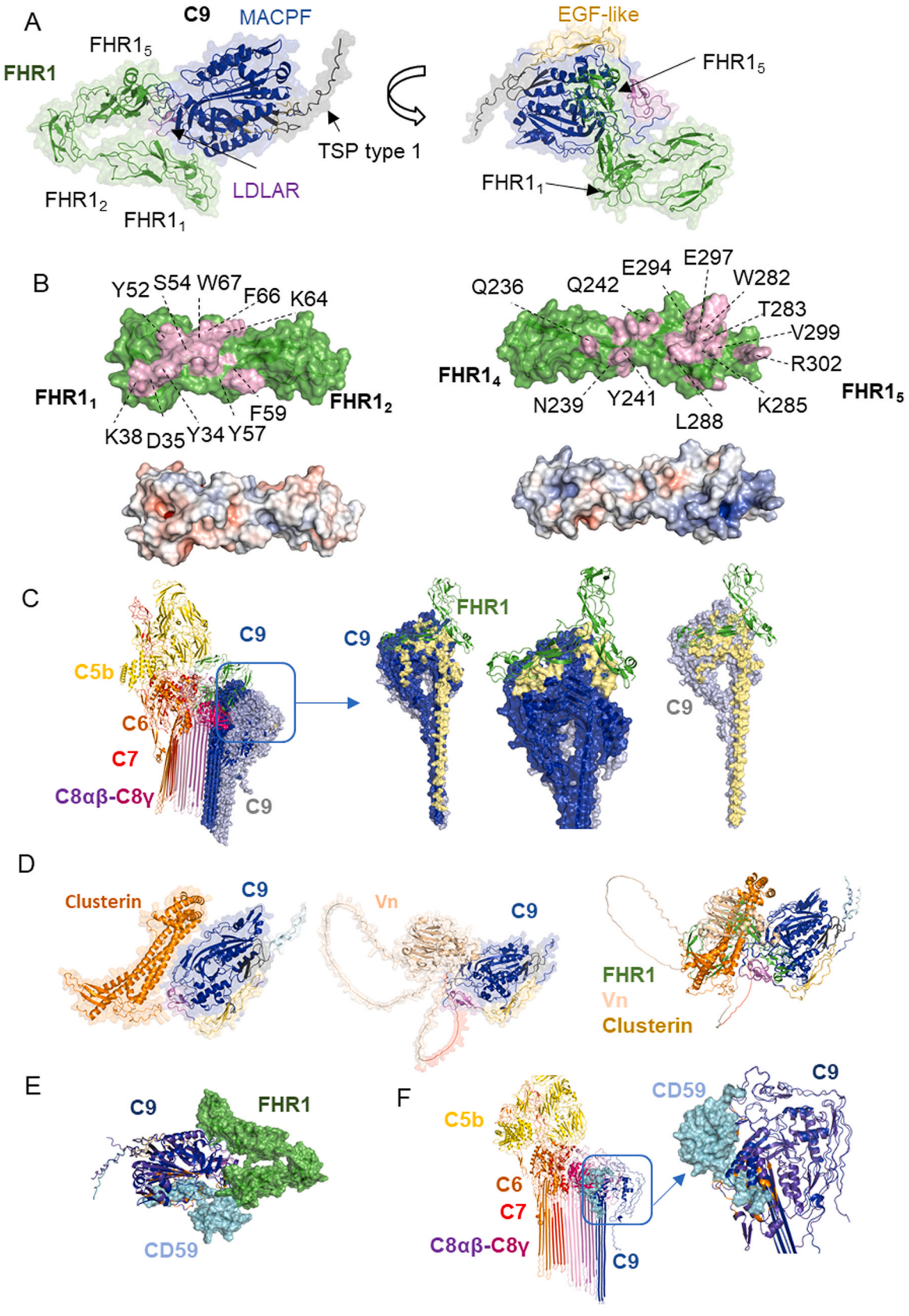

(caption on next page)

Fig. 6. Interactions between FHR1 and C9 predicted by AlphaFold Multimer **A.** $FHR1_{1-2}$ and $FHR1_5$ interact with C9 MACPF domain according to AFM model. FHR1 is shown in green and the colours of C9 domains match the colour of their legends. **B.** Binding interfaces of the model presented in A with electrostatic potential surface (electropositive and electronegative residues in blue and red, respectively). Some of the residues forming the binding region are labelled in FHR1. **C.** Interactions of vitronectin and clusterin with C9 predicted by AFM and superimposition of all models including FHR1 complex, suggest similar binding sites (only one of the top-ranked models is presented) **D.** FHR1 binding to C9 avoids C9 polymerization. Superimposition of C9 and FHR1 model with experimental structure of MAC (PDB 7nyc) is shown with a zoom in of interfaces between C8α -C9 and C9-C9, contrasted with binding sites of FHR1 (green) to C9 (blue and grey) in pale yellow. **E.** Interactions between membrane-anchored MAC regulator CD59 (shown in cyan) and C9 (dark blue) predicted by AFM are located in a buried region of soluble C9. The binding site is different from the predicted binding site for FHR1 (shown in green) **F.** Superimposition of AF2 model and experimental structure of MAC (PDB 7nyc) shows binding sites of CD59 in a hydrophobic pocket where unfurling of transmembrane β-hairpins occurs (binding sites in orange, soluble C9 and MAC C9 in purple and blue respectively). (For interpretation of the references to colour in this figure legend, the reader is referred to the web version of this article.)

individual TCC proteins C7, C8β and C9, but not C5, C6, C8α and C8γ [67]. Here, we also included a model of these complement regulators in complex with C9 and compared them with FHR1. According to the models predicted by AFM, Vn interacts with C9 mainly by a hydrophobic region which involves Trp 424, Trp 322 and Tyr 420 in Vn and Ile 203, Trp 197 and Arg 116 in C9, along with electrostatic interactions and hydrogen bonds (Supplementary Figure 7 B). On the other hand, clusterin interacts with C9 mainly by electrostatic interactions (including salt bridges) which involve Asp 178, Asp 174 and Glu 189 in clusterin and Arg 145, Arg 183 and Lys 114, along with hydrogen bonds (Supplementary Figure 7 C, D). Some of the key residues in the binding interface between C9 and Vn are some of those involved in hydrophobic interactions, while key residues in the interface with clusterin correspond to those involved in electrostatic interactions (Fig. 6 D). These models are congruent with previous experimental results indicating that Vn binds to a hydrophobic region of C9, while clusterin interacts with a charged patch in C9 [61].

The binding interfaces of clusterin, vitronectin and FHR1 are located in a similar region of the C9 MACPF domain where they interfere directly with binding to C5b-8 complex (Fig. 6 D). However, some of the top ranked models of clusterin showed additional binding sites (Supplementary Figure 7 E, F, G), which indicates that there are different interfaces on C9 for these regulators as suggested previously [61]. Furthermore, monomeric or polymerized C9 can compete with clusterin for the binding to C9 [68], which is congruent with our models of C9/FHR1 and C9/clusterin complexes, indicating that the binding interface coincide with the polymerization C9-C9 interface.

The regulator CD59 binds C8α and C9 in the C5b-8 or C5b-9 complexes during MAC assembly, preventing C9 binding and C9 polymerization, respectively [58,69]. Although the experimental structures of CD59 complexes with the complement components have not been reported, binding sites have been identified by peptide screening [69]. Therefore, we performed a prediction using AFM to evaluate whether it is congruent with the experimental data and compared it with FHR1 binding sites. A hydrophobic pocket in C9 was identified previously as the primary binding site for CD59 by docking models and mutagenesis studies [69–71], which is congruent with AFM prediction (Fig. 6 E, Supplementary Figure 7 H). This region is buried within C9 β-hairpins and undergoes a conformational change when C9 binds to the membrane-bound C5b-8 or C5b-9 complexes. Since CD59 cannot bind soluble C9, it should bind during the conformational rearrangement of transmembrane helices, and it might also prevent the complete conformational change (Fig. 6 F). Furthermore, the CD59 binding site could generate clashes with the C8γ subunit, therefore CD59 would not bind to the first C9 molecule recruited to the C5b-8 complex. Since the recruitment and insertion of the first C9 was recognized as the rate-limiting step in MAC formation [59], CD59 can act initially by binding to C8α chain to prevent bilayer perforation and C5b-9 complex formation. But once this complex is formed, CD59 binds to subsequent C9 in the complex to prevent further oligomerization. According to our AFM models, CD59 and C9 interact mainly by hydrophobic interactions with a binding region located in the transmembrane helices of C9, which include the peptide VSLAFS identified in C9 by experimental approaches [69]. Key residues in the interface include Phe 391, Phe 400, Phe 455, Phe 450, Val 452 in C9 and Phe 119, Leu 115, Leu 120, Trp 124, Pro 118 in CD59. CD59 might interfere with $FHR1_5$ interaction with C9 by steric hindrances but its binding site does not overlap with the binding region of $FHR1_1$. Therefore, our models indicate that CD59 might not compete with FHR1 (Fig. 6 E).

Although the confidence scores of the models between complement regulators such as clusterin, vitronectin, CD59 with C7 or C9 (inter-chain predicted alignment error) are lower than those for FHR1/C3d complexes, binding interfaces predicted by AFM are in agreement with experimental observations. Lower confidence scores were also obtained for all models between FHR1 in complex with C5, C7 or C9 than those for FHR1/C3d (Supplementary Table 1, Supplementary Figures 5, 6 A, 7 A), although we have experimentally measured a higher K_d for C5, C9 and C7 than for C3d in case of MFHR13, closely related to FHR1 [13]. Our models suggest that FHR1 competes with itself due to the dimerization interface for binding to C9. Moreover, it would compete with other ligands such as C3, C3b, C3d for binding to C5, C7 or C9. These findings might explain why FHR1 needed molar excess in respect to TCC proteins to inhibit MAC on sheep erythrocytes [13]. Although FHR1 and MAC components would probably not interact under normal conditions in plasma, local concentrations are higher on cell surfaces where complement is activated and FHR1 would interact with MAC proteins in the microenvironment of complement activation, which is especially relevant during infection.

As Alphafold-Multimer version 1 (AFM-v1) results frequently in clashes between protein chains, ColabFold also implemented an improved version, AFM version 2 (AFM-v2) [72]. All results presented here were obtained using AFM-v2. However, we compared both versions to predict FHR1 in complex with C5, C7, C9 and C3d using different recycle numbers. Increasing the recycle number has a severe impact in AFM-v1 confidence scores compared with AFM-v2. AFM-v1 and AFM-v2 correctly predicted binding interfaces in the complex FHR1/C3d, but we always observed higher confidence model scores for AFM-v1 prediction (pLDDT, pTM and iptm), including FHR1 in complex with C5, C7 and C9 (Supplementary Table 1). However, prediction with AFM-v1 led always to clashes in the case of the C5/FHR1 complex, and in some cases also for C7 and C9. We included an additional top-ranked model obtained with AFM-v1 that was ranked as the best predicted for the C9/FHR1 complex in which we did not detect clashes and suggested potential binding interfaces in a different region of C9 compared with AFM-v2 (Supplementary Figure 8 A). In that case, $FHR1_1$ binds to a region of C9 MACPF that undergoes a conformational change to insert into the membrane, indicating that FHR1 would interfere with the conformational change of C9 upon C5b-8 binding (Supplementary Figure 8 B). The models from the two different versions are not contradictory, as several potential binding sites of FHR1 are possible for these TCC proteins as in the case of clusterin and vitronectin.

Furthermore, our models predicted binding interfaces in $FHR1_{1-2}$ or $FHR1_{4-5}$ with C5, C7 and C9. It is important to mention that MFHR13 includes $FHR1_{1-2}$ and FH_{19-20}, which differ from $FHR1_{4-5}$ only by two residues (SV in FH_{20} and LA in $FHR1_5$). Nevertheless, we have not detected binding of FH to these proteins in wet lab experiments [13]. These differences have important implications for

the mechanism of action of both proteins; the SV motif (FH) binds efficiently to sialic acids contrary to the LA motif (FHR1) [10]. These differences might explain previous results where MFHR13 protected more efficiently C3b-opsonized sheep erythrocytes from convertase-independent C5 activation and MAC formation than FHR1 [13], as MFHR13 ($FHR1_{1-2}$:FH_{1-4}:FH_{13}:FH_{19-20}) would bind more efficiently to the sialic acid-rich surface of sheep erythrocytes, regulating MAC formation on the cell surface. Furthermore, FH binds more efficiently to heparin-C3b while FHR1 binds better to a heparin-C3d combination [73]. Although in none of our models Leu 290 or Ala 296 were identified as key residues in the binding interfaces of FHR1, the effect of these motifs (SV and LA, on FH and FHR1, resp.) on the binding capacity to C3b/C3d, C5, C7 and C9 should be experimentally investigated, to validate the binding interfaces in $FHR1_{4-5}$ and to elucidate if the inability of FH to bind to C5, C7 and C9 depends on the sequence of FH_{20} or on the conformation of FH in fluid phase.

The role of FHR1 as a MAC complement regulator has been controversial. However, it has been proposed that FHR1 acts either as complement regulator or "FH antagonist" depending on the context [74,75]. For instance, the knockout of the murine FHR1 homolog resulted in mice with severe sepsis, acute kidney injury and alternative pathway overactivation in response to LPS challenge [76]. Therefore, under physiological conditions, FHR1 could promote complement opsonization on damaged host cells to facilitate phagocytosis, while preventing MAC formation and restricting inflammation. In case of complement overactivation during disease, FHR1 might act as MAC regulator.

3. Conclusion

Here we used AF2 and AFM to predict the structures of synthetic and native human complement regulators and provide insights into their molecular interactions with complement components. Differences in MFHR1 and MFHR13 structures explain differences in alternative pathway regulation observed experimentally before, supporting these results [13]. However, these models should be interpreted with caution, since domain orientation is still difficult to predict. AFM predicted successfully binding interfaces of FHR1 and the synthetic regulators to C3b and C3d. According to this study, the synthetic regulators might even interact with C3, a feature that had not been previously considered, and its impact on complement regulation should be evaluated.

Here, we generated various hypotheses based on AF2/AFM structural and binding predictions to understand the molecular mechanisms of complement regulation, with emphasis on MAC inhibition. AFM predicted binding interfaces between Vn, clusterin, and CD59 with C7 and C9, which coincide with some experimental observations, although the binding interfaces and key residues still need to be determined for Vn and clusterin. These may serve as basis to design straightforward experiments using a rational approach to identify binding interfaces of MAC proteins C5, C7, and C9 with natural regulators (FHR1, clusterin or Vn) or synthetic regulators (MFHR1 or MFHR13). For example, potential binding interfaces predicted by AFM could be confirmed by binding experiments, like Surface Plasmon Resonance (SPR), Biolayer Interferometry (BLI) or Microscale Thermophoresis (MST), using site-directed mutagenesis of postulated key residues or peptide screening. According to AFM predicted structures, we propose that binding of FHR1 to C5 might partially block C3b binding located in the C5 CUB domain, inhibiting in turn C5 activation, which should be experimentally validated using for example competition assays in SPR or MST. AFM-predicted models suggest that FHR1 binding to C7 and C9 would interfere with C5b-7 formation and C9 polymerization. Furthermore, FHR1 binding to C5, C7 or C9 would compete with other ligands such as C3, C3b, C3d, due to binding interfaces predicted in $FHR1_{4-5}$, which was unexpected due to their high similarity to FH_{19-20}. Therefore, it is important to validate this binding interface using initially recombinant fragments of $FHR1_{4-5}$.

The clinical relevance of FHR1 interactions with MAC components cannot be predicted yet. However, understanding protein-protein interactions in the context of complement regulation is fundamental to understand complement-associated diseases and develop novel therapeutics. In this sense, AF2/AFM can be a powerful tool as a starting point to unravel complement regulatory mechanisms. For example, several pathogens have evolved to evade attack of the complement system, among them *Neissseria meningiditis, Borrelia miyamotoi*, *Yersinia* and *Salmonella* species which can recruit FH or Vn to their surface [77,78]. Prediction of such interactions via AF2/AFM would simplify unveiling mechanisms of immune evasion and might lead to targeted treatments.

4. Methods

4.1 Prediction of protein structures protein-protein interactions

The sequences of complement proteins were retrieved from UniProt. To predict protein structures, we used Colabfold [29], which is based on the AlphaFold2 (AF2) algorithm to predict monomers [27] and AlphaFold-Multimer [28] to predict protein complexes. ColabFold uses MMseqs2 (Many-against-Many sequence searching) instead of AF2 homology search (HMMer and HHblits), which significantly accelerates the prediction, while matching the prediction quality [29].

We used local ColabFold, a free open-source software, which allows to run ColabFold in our local machines instead of Google Colaboratory. We run ColabFold in Linux with Nvidia GPU V100 (CUDA 11.1 was installed). All models were run using amber relaxation, important for the positioning of the side chains and to avoid steric clashes. The number of recycles was modified from the default settings. This is the number of times the prediction is fed through the model what may improve the quality significantly [29]. Although 3 is used by default, we also included 6, 8, 12 and 20 recycles. We used templates for the protein complexes in PDB70 and compared them with models generated without templates.

ColabFold implemented two algorithms to predict protein-complexes based on AlphaFold-multimer (AFM) version 1 and 2 [28,29]. AF2/AFM computes five models for every run and we analysed the models with the best score across all runs with variable recycle number. AF2 model quality is evaluated using two metrics, the predicted Local Distance Difference Test (pLDDT) and predicted Aligned Error (PAE). For protein complexes, inter-chain PAE and interface pTM score (iptm) was used to evaluate the accuracy of interfaces and model confidence. Inter-chain PAE plots are shown in supplementary data. High and low prediction quality are indicated in blue (values close to 0) and red (values close to 30), respectively.

The quality of the synthetic regulator (MFHR1 and MFHR13) models were additionally evaluated using Ramachandran Plot in PROCHECK module implemented in SAVES server to analyse stereochemical quality (https://saves.mbi.ucla.edu/), and QMEANDisCo [35] (https://swissmodel.expasy.org/qmean/).

4.2 Other tools

We used Pymol 2.5.4 (Schrödinger, LLC, New York, NY, USA) to visualize and analyse the 3D protein structures including analysis of interactions between proteins (using the plugins show_contacts, list_contacts), calculation of electrostatic surface potential, and root-mean-square deviation of atomic positions (RMSD) to compare the predictions with experimental structures by structural alignment (alignment /superposition plugin). The experimental protein structures were retrieved from the RCSB protein data Bank (https://www.rcsb.org/). The following PDB structures were used for

analysis: PDB 2wii (complex FH_{1-4}/C3b), PDB complex mini-FH: C3b (5035), PDB 2a73 (C3), PDB 2xqw (C3d/FH_{19-20}), PDB 4muc, 3rj3 (C3d/$FHR1_{4-5}$), PDB 7nyc (soluble MAC with 3C9), PDB 2kms (FH_{12-13}), PDB 3sw0 (FH_{18-20}), PDB 2win (C3 convertase C3bBb), PDB 4ont (C3d/sialic acid/FH_{19_20}), PDB 3zd2 (dimer $FHR1_{1-2}$), PDB 4e0s (C5b6).

Intermolecular interactions, bumps and clashes were also analysed using BIOVIA Discovery Studio Visualizer 21.0.0 (Biovia Dassault Systèmes, San Diego, USA). Other model features such as hydrophobic clusters were analysed using ProteinTools web server [79].

The intrinsic disordered regions were identified with the following web tools: IUPred2A [80], DISOPRED3 [81], fMoRFpred [82], DFLpred [83] and TransDFL [84].

Binding free energy of the best models was calculated using molecular mechanics/generalized Born surface area (MM/GBSA) method implemented in HawkDock server to identify key residues in the binding interfaces [85].

Authorship contribution statement

NR-M: Conceptualization, Methodology, Formal analysis, Writing – original draft preparation. **JP:** Conceptualization, Writing – original draft preparation. **ELD:** Funding acquisition, Writing – reviewing and editing. **RR:** Conceptualization, Funding acquisition, Writing – reviewing and editing. All authors read and approved the final manuscript.

Declaration of Competing Interest

All authors declare to have no competing interests.

Acknowledgements

This work was supported by the Mathias-Tantau-Stiftung (to NR-M) and the Deutsche Forschungsgemeinschaft (DFG, German Research Foundation) under Germany's Excellence Strategy EXC-2189 (CIBSS; to RR). We thank the German Network for Bioinformatics Infrastructure (de.NBI) for the computational resources, Andres Posada Moreno for his help with setting up the servers, Anne Katrin Prowse for proof-reading of the manuscript, and Michal Rössler/CIBSS graphics for her help with the graphical abstract.

References

[1] Zipfel PF, Skerka C. Complement regulators and inhibitory proteins. Nat Rev Immunol 2009;9:729–40.
[2] Chen ZA, Pellarin R, Fischer L, Sali A, Nilges M, Barlow PN, et al. Structure of complement C3(H2O) revealed by quantitative cross-linking/mass spectrometry and modeling. Mol Cell Proteom 2016;15:2730–43.
[3] Ricklin D, Reis ES, Mastellos DC, Gros P, Lambris JD. Complement component C3 – The "Swiss Army Knife" of innate immunity and host defense. Immunol Rev 2016;274:33–58.
[4] Mannes M, Dopler A, Zolk O, Lang SJ, Halbgebauer R, Höchsmann B, et al. Complement inhibition at the level of C3 or C5: Mechanistic reasons for ongoing terminal pathway activity. Blood 2021;137:443–55.
[5] Bayly-Jones C, Bubeck D, Dunstone MA. The mystery behind membrane insertion: a review of the complement membrane attack complex. Philos Trans R Soc B Biol Sci 2017:372.
[6] Merle NS, Church SE, Fremeaux-Bacchi V, Roumenina LT. Complement system part I - molecular mechanisms of activation and regulation. Front Immunol 2015;6:262.
[7] Harboe M, Ulvund G, Vien L, Fung M, Mollnes TE. The quantitative role of alternative pathway amplification in classical pathway induced terminal complement activation. Clin Exp Immunol 2004;138:439–46.
[8] Kajander T, Lehtinen MJ, Hyvärinen S, Bhattacharjee A, Leung E, Isenman DE, et al. Dual interaction of factor H with C3d and glycosaminoglycans in host-nonhost discrimination by complement. Proc Natl Acad Sci USA 2011;108:2897–902.
[9] Goicoechea de Jorge E, Caesar JJE, Malik TH, Patel M, Colledge M, Johnson S, et al. Dimerization of complement factor H-related proteins modulates complement activation in vivo. Proc Natl Acad Sci USA 2013;110:4685–90.
[10] Dopler A, Stibitzky S, Hevey R, Mannes M, Guariento M, Höchsmann B, et al. Deregulation of factor H by factor h-related protein 1 depends on sialylation of host surfaces. Front Immunol 2021;12:201.
[11] Merinero HM, Subías M, Pereda A, Gómez-Rubio E, Juana Lopez L, Fernandez C, et al. Molecular bases for the association of FHR-1 with atypical hemolytic uremic syndrome and other diseases. Blood 2021;137:3484–94.
[12] Heinen S, Hartmann A, Lauer N, Wiehl U, Dahse H-M, Schirmer S, et al. Factor H–related protein 1 (CFHR-1) inhibits complement C5 convertase activity and terminal complex formation. Blood 2009;114:2439–47.
[13] Ruiz-Molina N, Parsons J, Müller M, Hoernstein SNW, Bohlender LL, Pumple S, et al. A synthetic protein as efficient multitarget regulator against complement over-activation. Commun Biol 2022;5:152.
[14] Gralinski LE, Sheahan TP, Morrison TE, Menachery VD, Jensen K, Leist SR, et al. Complement activation contributes to severe acute respiratory syndrome coronavirus pathogenesis. MBio 2018;9. e01753-18.
[15] Carr JM, Cabezas-Falcon S, Dubowsky JG, Hulme-Jones J, Gordon DL. Dengue virus and the complement alternative pathway. FEBS Lett 2020;594:2543–55.
[16] Kittlesen DJ, Chianese-Bullock KA, Yao ZQ, Braciale TJ, Hahn YS. Interaction between complement receptor gC1qR and hepatitis C virus core protein inhibits T-lymphocyte proliferation. J Clin Invest 2000;106:1239–49.
[17] Gao T, Zhu L, Liu H, Zhang X, Wang T, Fu Y, et al. Highly pathogenic coronavirus N protein aggravates inflammation by MASP-2-mediated lectin complement pathway overactivation. Signal Transduct Target Ther 2022;7:318.
[18] Ricklin D, Reis ES, Lambris JD. Complement in disease: a defence system turning offensive. Nat Rev Nephrol 2016;12:383–401.
[19] Banerjee P, Veuskens B, de Jorge EG, Józsi M, Baeumner AJ, Steiner MS, et al. Evaluating the clinical utility of measuring levels of factor H and the related proteins. Mol Immunol 2022;151:166–82.
[20] Büttner-Mainik A, Parsons J, Jérôme H, Hartmann A, Lamer S, Schaaf A, et al. Production of biologically active recombinant human factor H in Physcomitrella. Plant Biotechnol J 2011;9:373–83.
[21] Michelfelder S, Parsons J, Bohlender LL, Hoernstein SNW, Niederkrüger H, Busch A, et al. Moss-produced, glycosylation-optimized human Factor H for therapeutic application in complement disorders. J Am Soc Nephrol 2017;28:1462–74.
[22] Hebecker M, Alba-Domínguez M, Roumenina LT, Reuter S, Hyvärinen S, Dragon-Durey M-A, et al. An engineered construct combining complement regulatory and surface-recognition domains represents a minimal-size functional factor H. J Immunol 2013;191:912–21.
[23] Schmidt CQ, Bai H, Lin Z, Risitano AM, Barlow PN, Ricklin D, et al. Rational engineering of a minimized immune inhibitor with unique triple targeting properties. J Immunol 2013;190:5712–21.
[24] Nichols EM, Barbour TD, Pappworth IY, Wong EKS, Palmer JM, Sheerin NS, et al. An extended mini-complement factor H molecule ameliorates experimental C3 glomerulopathy. Kidney Int 2015;88:1314–22.
[25] Michelfelder S, Fischer F, Wäldin A, Hörle KV, Pohl M, Parsons J, et al. The MFHR1 fusion protein is a novel synthetic multitarget complement inhibitor with therapeutic potential. J Am Soc Nephrol 2018;29:1141–53.
[26] Top O, Parsons J, Bohlender LL, Michelfelder S, Kopp P, Busch-Steenberg C, et al. Recombinant production of mfhr1, a novel synthetic multitarget complement inhibitor, in moss bioreactors. Front Plant Sci 2019;10:260.
[27] Jumper J, Evans R, Pritzel A, Green T, Figurnov M, Ronneberger O, et al. Highly accurate protein structure prediction with AlphaFold. Nature 2021;596:583–9.
[28] Evans R, O'Neill M, Pritzel A, Antropova N, Senior A, Green T, et al. Protein complex prediction with AlphaFold-Multimer. BioRxiv 2022. https://doi.org/10.1101/2021.10.04.463034
[29] Mirdita M, Schütze K, Moriwaki Y, Heo L, Ovchinnikov S, Steinegger M. ColabFold: making protein folding accessible to all. Nat Methods 2022;19:679–82.
[30] Yin R, Feng BY, Varshney A, Pierce BG. Benchmarking AlphaFold for protein complex modeling reveals accuracy determinants. Protein Sci 2022;31:e4379.
[31] Bryant P, Pozzati G, Elofsson A. Improved prediction of protein-protein interactions using AlphaFold2. Nat Commun 2022;13:1265.
[32] Chowdhury R, Bouatta N, Biswas S, Floristean C, Kharkar A, Roy K, et al. Single-sequence protein structure prediction using a language model and deep learning. Nat Biotechnol 2022;40:1617–23.
[33] Ruff KM, Pappu RV. AlphaFold and implications for intrinsically disordered proteins. J Mol Biol 2021;433:167208.
[34] Schmidt CQ, Herbert AP, Mertens HDT, Guariento M, Soares DC, Uhrin D, et al. The central portion of factor H (modules 10–15) is compact and contains a structurally deviant CCP module. J Mol Biol 2010;395:105.
[35] Studer G, Rempfer C, Waterhouse AM, Gumienny R, Haas J, Schwede T. QMEANDisCo—distance constraints applied on model quality estimation. Bioinformatics 2020;36:1765–71.
[36] Janssen BJC, Huizinga EG, Raaijmakers HCA, Roos A, Daha MR, Nilsson-Ekdahl K, et al. Structures of complement component C3 provide insights into the function and evolution of immunity. Nature 2005;437:505–11.
[37] Wu J, Wu YQ, Ricklin D, Janssen BJC, Lambris JD, Gros P. Structure of C3b-factor H and implications for host protection by complement regulators. Nat Immunol 2009;10:728–33.
[38] Morgan HP, Schmidt CQ, Guariento M, Blaum BS, Gillespie D, Herbert AP, et al. Structural basis for engagement by complement factor H of C3b on a self surface. Nat Struct Mol Biol 2011;18:463–70.

[39] Haque A, Cortes C, Alam MN, Sreedhar M, Ferreira VP, Pangburn MK. Characterization of binding properties of individual functional sites of human complement factor H. Front Immunol 2020;11:1728.
[40] Morgan HP, Mertens HDT, Guariento M, Schmidt CQ, Soares DC, Svergun DI, et al. Structural analysis of the C-terminal region (Modules 18–20) of complement regulator Factor H (FH). PLoS One 2012;7:32187.
[41] Schmidt CQ, Harder MJ, Nichols EM, Hebecker M, Anliker M, Höchsmann B, et al. Selectivity of C3-opsonin targeted complement inhibitors: a distinct advantage in the protection of erythrocytes from paroxysmal nocturnal hemoglobinuria patients. Immunobiology 2016;221:503–11.
[42] Janssen BJC, Christodoulidou A, McCarthy A, Lambris JD, Gros P. Structure of C3b reveals conformational changes that underlie complement activity. Nature 2006;444:213–6.
[43] Zhou X, Peng C, Zheng W, Li Y, Zhang G, Zhang Y. DEMO2: Assemble multi-domain protein structures by coupling analogous template alignments with deep-learning inter-domain restraint prediction. Nucleic Acids Res 2022;50:W235–45.
[44] van Breugel M. Rosa e Silva I, Andreeva A. Structural validation and assessment of AlphaFold2 predictions for centrosomal and centriolar proteins and their complexes. Commun Biol 2022;5:312.
[45] Wilson CJ, Choy WY, Karttunen M. AlphaFold2: a role for disordered protein/region prediction? Int J Mol Sci 2022;23:4591.
[46] Noris M, Remuzzi G. Overview of complement activation and regulation. Semin Nephrol 2013;33:479–92.
[47] Roversi P, Johnson S, Caesar JJE, McLean F, Leath KJ, Tsiftsoglou SA, et al. Structural basis for complement factor I control and its disease-associated sequence polymorphisms. Proc Natl Acad Sci USA 2011;108:12839–44.
[48] Harder MJ, Anliker M, Höchsmann B, Simmet T, Huber-Lang M, Schrezenmeier H, et al. Comparative analysis of novel complement-targeted inhibitors, miniFH, and the natural regulators Factor H and Factor H-like protein 1 reveal functional determinants of complement regulation. J Immunol 2016;196:866–76.
[49] Papp A, Papp K, Uzonyi B, Cserhalmi M, Csincsi ÁI, Szabó Z, et al. Complement Factor H-related proteins FHR1 and FHR5 interact with extracellular matrix ligands, reduce Factor H regulatory activity and enhance complement activation. Front Immunol 2022;13:935.
[50] Rooijakkers SHM, Wu J, Ruyken M, van Domselaar R, Planken KL, Tzekou A, et al. Structural and functional implications of the alternative complement pathway C3 convertase stabilized by a staphylococcal inhibitor. Nat Immunol 2009;10:721–7.
[51] Bhattacharjee A, Reuter S, Trojnár E, Kolodziejczyk R, Hyvärinen HSS, Uzonyi B, et al. The major autoantibody epitope on Factor H in atypical hemolytic uremic syndrome is structurally different from its homologous site in Factor H-related protein 1, supporting a novel model for induction of autoimmunity in this disease. J Biol Chem 2015;290:9500–10.
[52] Jore MM, Johnson S, Sheppard D, Barber NM, Li YI, Nunn MA, et al. Structural basis for therapeutic inhibition of complement C5. Nat Struct Mol Biol 2016;23(378–86).
[53] Hadders MA, Bubeck D, Roversi P, Hakobyan S, Forneris F, Morgan BP, et al. Assembly and regulation of the membrane attack complex based on structures of C5b6 and sC5b9. Cell Rep 2012;1:200–7.
[54] Zipfel PF, Wiech T, Gröne HJ, Skerka C. Complement catalyzing glomerular diseases. Cell Tissue Res 2021;385:355–70.
[55] Macpherson A, Laabei M, Ahdash Z, Graewert M, Birtley JR, Schulze MSED, et al. The allosteric modulation of complement C5 by knob domain peptides. Elife 2021;10:e63586.
[56] Macpherson A, Liu X, Dedi N, Kennedy J, Carrington B, Durrant O, et al. The rational design of affinity-attenuated OmCI for the purification of complement C5. J Biol Chem 2018;293:14112–21.
[57] Laursen NS, Andersen KR, Braren I, Spillner E, Sottrup-Jensen L, Andersen GR. Substrate recognition by complement convertases revealed in the C5–cobra venom factor complex. EMBO J 2011;30:606–16.
[58] Naughton MA, Walport MJ, Würzner R, Carter MJ, Alexander GJM, Goldman JM, et al. Organ-specific contribution to circulating C7 levels by the bone marrow and liver in humans. Eur J Immunol 1996;26:2108–12.
[59] Parsons ES, Stanley GJ, Pyne ALB, Hodel AW, Nievergelt AP, Menny A, et al. Single-molecule kinetics of pore assembly by the membrane attack complex. Nat Commun 2019;10:2066.
[60] Menny A, Serna M, Boyd CM, Gardner S, Joseph AP, Morgan BP, et al. CryoEM reveals how the complement membrane attack complex ruptures lipid bilayers. Nat Commun 2018;9:5316.
[61] Menny A, Lukassen MV, Couves EC, Franc V, Heck AJR, Bubeck D. Structural basis of soluble membrane attack complex packaging for clearance. Nat Commun 2021;12:6086.
[62] Yorulmaz S, Jackman JA, Hunziker W, Cho NJ. Supported lipid bilayer platform to test inhibitors of the membrane attack complex: insights into biomacromolecular assembly and regulation. Biomacromolecules 2015;16:3594–602.
[63] Tschopp J, Masson D, Schäfer S, Peitsch M, Preissner KT. The heparin binding domain of S-protein/vitronectin binds to complement components C7, C8, and C9 and perforin from cytolytic T-cells and inhibits their lytic activities. Biochemistry 1988;27:4103–9.
[64] Sheehan M, Morris CA, Pussell BA, Charlesworth JA. Complement inhibition by human vitronectin involves non-heparin binding domains. Clin Exp Immunol 1995;101:136–41.
[65] Erijman A, Rosenthal E, Shifman JM. How structure defines affinity in protein-protein interactions. PLoS One 2014;9:e110085.
[66] Milis L, Morris CA, Sheehan MC, Charlesworth JA, Pussell BA. Vitronectin-mediated inhibition of complement: evidence for different binding sites for C5b-7 and C9. Clin Exp Immunol 1993;92:114–9.
[67] Tschopp J, Chonn A, Hertig S, Frencht LEClusterin. the human apolipoprotein and complement inhibitor, binds to complement C7, CSP, and the b domain of C9. J Immunol 1993;151:2159–65.
[68] McDonald JF, Nelsestuen GL. Potent inhibition of terminal complement assembly by clusterin: characterization of its impact on C9 polymerization. Biochemistry 1997;36:7464–73.
[69] Huang Y, Qiao F, Abagyan R, Hazard S, Tomlinson S. Defining the CD59-C9 binding interaction. J Biol Chem 2006;281:27398–404.
[70] Yu J, Dong S, Rushmere NK, Morgan BP, Abagyan R, Tomlinson S. Mapping the regions of the complement inhibitor CD59 responsible for its species selective activity. Biochemistry 1997;36:9423–8.
[71] Zhao XJ, Zhao J, Zhou Q, Sims PJ. Identity of the residues responsible for the species-restricted complement inhibitory function of human CD59. J Biol Chem 1998;273:10665–71.
[72] Bryant P, Pozzati G, Zhu W, Shenoy A, Kundrotas P, Elofsson A. Predicting the structure of large protein complexes using AlphaFold and Monte Carlo tree search. Nat Commun 2022;13:6028.
[73] Perie L, Stippa S, Hartmann A, Mihlan M, Skerka C, Wiech T, et al. The three C-terminal domains of FHR1 influence complement activation and FHR1 co-operation with other complement regulators. Kidney Int Rep 2022;7:S437–8.
[74] Skerka C, Pradel G, Halder LD, Zipfel PF, Zipfel SLH, Strauß O. Factor H-related protein 1: a complement regulatory protein and guardian of necrotic-type surfaces. Br J Pharm 2021;178:2823–31.
[75] Li X, Zong J, Si S. Complement Factor H related protein 1 and immune inflammatory disorders. Mol Immunol 2022;145:43–9.
[76] Li X, Hao Z, Liu X, Li W. Deficiency of mouse FHR-1 homolog, FHR-E, accelerates sepsis, and acute kidney injury through enhancing the LPS-induced alternative complement pathway. Front Immunol 2020;11:1123.
[77] Walter L, Sürth V, Röttgerding F, Zipfel PF, Fritz-Wolf K, Kraiczy P. Elucidating the immune evasion mechanisms of *Borrelia mayonii*, the causative agent of Lyme disease. Front Immunol 2019;10:2722.
[78] Krukonis ES, Thomson JJ. Complement evasion mechanisms of the systemic pathogens Yersiniae and Salmonellae. FEBS Lett 2020;594:2598–620.
[79] Ferruz N, Schmidt S, Höcker B. ProteinTools: a toolkit to analyze protein structures. Nucleic Acids Res 2021;49:W559–66.
[80] Mészáros B, Erdös G, Dosztányi Z. IUPred2A: context-dependent prediction of protein disorder as a function of redox state and protein binding. Nucleic Acids Res 2018;46:W329–37.
[81] Jones DT, Cozzetto D. DISOPRED3: precise disordered region predictions with annotated protein-binding activity. Bioinformatics 2015;31:857–63.
[82] Yan J, Dunker AK, Uversky VN, Kurgan L. Molecular recognition features (MoRFs) in three domains of life. Mol Biosyst 2016;12:697–710.
[83] Meng F, Kurgan L. DFLpred: High-throughput prediction of disordered flexible linker regions in protein sequences. Bioinformatics 2016;32:i341–50.
[84] Pang Y, Liu B. TransDFL: identification of disordered flexible linkers in proteins by transfer learning. Genomics Proteomics Bioinformatics. In press,; 2022.
[85] Weng G, Wang E, Wang Z, Liu H, Zhu F, Li D, et al. HawkDock: a web server to predict and analyze the protein–protein complex based on computational docking and MM/GBSA. Nucleic Acids Res 2019;47:W322–30.